Applied Catalysis B: Environmental 129 (2013) 194–201

Contents lists available at SciVerse ScienceDirect

Applied Catalysis B: Environmental

journal homepage: www.elsevier.com/locate/apcatb

Highly efficient bacteria inactivation and phenol degradation by visible light irradiated iodine doped TiO_2

G. Veréb[a], L. Manczinger[b], A. Oszkó[c], A. Sienkiewicz[d], L. Forró[d], K. Mogyorósi[a,*], A. Dombi[a], K. Hernádi[a]

[a] Research Group of Environmental Chemistry, Institute of Chemistry, University of Szeged, H-6720 Szeged, Dom ter 7, Hungary
[b] Department of Microbiology, Faculty of Sciences and Informatics, University of Szeged, H-6701 Szeged, P.O. Box 533, Hungary
[c] Department of Physical Chemistry and Material Science, Faculty of Sciences and Informatics, University of Szeged, H-6720 Szeged, P.O. Box 168, Hungary
[d] FSB, IPMC, LPMC, Station 3, Ecole Polytechnique Fédérale de Lausanne, CH-1015 Lausanne, Switzerland

ARTICLE INFO

Article history:
Received 4 June 2012
Received in revised form 28 August 2012
Accepted 30 August 2012
Available online 7 September 2012

Keywords:
Photocatalysis
Iodine doped
Visible light
Disinfection
Escherichia coli
Titanium dioxide
Spin trapping

ABSTRACT

In this study visible light active iodine doped titanium dioxide samples prepared by sol–gel method were investigated. Photocatalysts were characterized by X-ray diffraction (XRD), transmission electron microscopy (TEM), X-ray fluorescence spectroscopy (XFS), diffuse reflectance spectroscopy (DRS), X-ray photoelectron spectroscopy (XPS) and by Brunauer–Emmett–Teller (BET) surface area technique.

Different iodine/titanium ratios (n_I/n_{Ti} = 0.0–2.6) were applied during the synthesis and the optimum value was determined by phenol degradation under UV and VIS irradiations. The photocatalytic efficiency towards phenol degradation and the inactivation of *Escherichia coli* (*E. coli*) contaminated water under visible light illumination (conventional 24 W energy-saving compact fluorescence lamps) of the most active iodine-doped TiO_2 (n_I/n_{Ti} = 0.5; 79.5 m^2/g; 98 wt% anatase) was compared with well known reference photocatalysts, that are Aeroxide P25 and Aldrich anatase (>85 nm primary crystallite size). Results showed that our iodine doped TiO_2 was far more efficient at inactivating the *E. coli* and decomposing the phenol than Aeroxide P25. Electron spin resonance (ESR) measurements confirmed the formation of highly reactive $OH^{\bullet}$ radicals by the iodine doped titania under VIS irradiation. In contrast, singlet oxygen and superoxide radical ions were not detected. The performed experiments also proved that dissolved iodine was produced in very low concentrations (about 0.01–0.025 mg/L) from the irradiated titanium dioxide. The dissolved iodine could have some contribution to the phenol oxidation and the disinfection effects. This study demonstrated this property of iodine-doped titanias for the first time.

1. Introduction

Looking for visible light active titanium dioxide based photocatalysts is nowadays an intensely investigated research area. In an economical and environmentally friendly photocatalysis based water treatment, solar radiation activates the photocatalyst. It is well known that in the solar spectrum the intensity of the light in the visible range is greater than in the UV range [1–4], consequently visible light active photocatalysts could be more efficient for solar photocatalysis. Moreover for indoor surface/air cleaning, only visible light active titanias are applicable due to the negligible number of UV photons under usual internal lighting conditions. To render titanium dioxide active under visible light, it was doped by several elements such as nitrogen [5–9], iron [10–12], sulphur [5,6,13], iodine [1,3,4,14–32], silver [1,7,33], *etc.* Hong et al. [4] were the first to publish on iodine doped, visible light active titanium dioxide in 2005. Recently, iodine doped titanium dioxide has received much attention. Before 2010 only a few articles on the subject were available [4,14,17–21,30], however in the last two years this number has increased significantly [3,15,16,22–29,31,32]. Many authors report that iodine doped titanias are highly efficient at decomposing organic pollutants such as phenols [3,4,15,20,26–28,31], methylene blue [14,17,23], oxalic acid [18,30], methyl orange [16,32], rhodamine B [26] and acetone [19] under visible light, but no studies in the literature could be found about the disinfection property of solely iodine doped titanias. In 2010, Jiang and co-workers [23] published that neodymium and iodine co-doped TiO_2 nanoparticles could inhibit *Escherichia coli* and *Staphylococcus aureus* through damaging their outer membranes by the irradiation of visible light. Furthermore in 2011 Shirai et al. [34] published a paper in which iodine-supported titanium was investigated as an antibacterial implant. Since the antibacterial activity of the photocatalysts is very important for applications in both drinking water production and for indoor air/surface cleaning, we present here a study

* Corresponding author at: Research Group of Environmental Chemistry, Institute of Chemistry, Faculty of Science and Informatics, University of Szeged, H-6720 Szeged, Tisza L. krt. 103, Hungary. Tel.: +36 62 544 334; fax: +36 62 420 505.
E-mail address: k.mogyorosi@chem.u-szeged.hu (K. Mogyorósi).

0926-3373/$ – see front matter © 2012 Elsevier B.V. All rights reserved.
http://dx.doi.org/10.1016/j.apcatb.2012.08.037

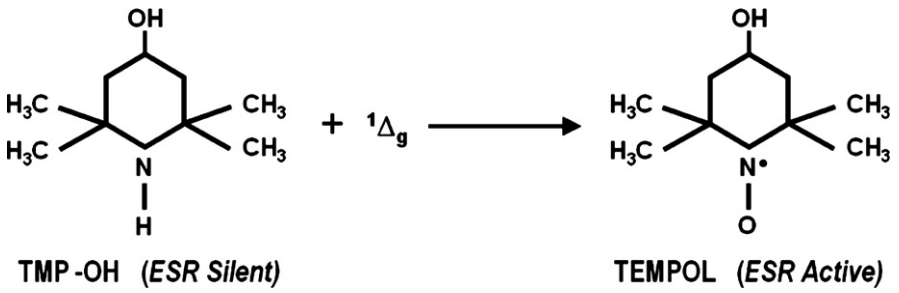

Scheme 1. Reactive scavenging of singlet oxygen ($^1O_2$) with TMP-OH.

which investigates the disinfection efficiency of visible light irradiated iodine doped titanium dioxide by *E. coli* inactivation, beside the phenol decomposition efficiency. Detailed characterization of the photocatalytic disinfection process with iodine doped titania was also an important goal of this work.

2. Experimental

2.1. Materials

Two well known nano-sized titanium dioxides were used as reference photocatalysts in this study. Aeroxide P25 (Evonik Industries, 10% rutile and 90% anatase, crystallite size ~25–40 nm), herein referred to as TiO_2–P25 and a pure anatase photocatalyst (Sigma–Aldrich, 100% anatase, average crystallite size ~ 85 nm) herein referred to as TiO_2–AA.

2.1.1. Synthesis of iodine doped TiO_2 photocatalysts

Iodine doped titanium dioxides were synthesized by the dropwise addition of titanium tetrabutoxide (Fluka, 97%) to iodic acid (Fluka, 99.5%) solution (c_{HIO3} = 0.15 M in Milli-Q water) following the method applied by Hong et al. [4]. Different iodine/titanium molar ratios were used during the hydrolysis of titanium tetrabutoxide which were 0.00, 0.10, 0.50, 1.30 and 2.60 in the dispersion. Samples were named in order of the molar ratios such that TiO_2-I-zero refers to 0.00, TiO_2-Ib to 0.10, TiO_2-Ic to 0.50, TiO_2-Id to 1.30 and TiO_2-Ie to 2.60. The suspensions were stirred for 1 hour and then dried at 100 °C. The powders were homogenized by milling in an agate mortar and calcinated in a tubular furnace at 400 °C for 2 hours, with 4 °C/min heating rate (air purging was applied). The samples were brownish yellow in colour, darkening at higher added iodic acid content. The powders were re-ground at room temperature.

2.2. Methods and instrumentation

X-ray diffraction (XRD) measurements were carried out on a Rigaku diffractometer (λCu Kα = 0.15406 nm, 30 kV, and 15 mA, in the 20–40° (2Θ) regime). Using the Scherrer equation the average diameters of the particles were derived. The weight fraction of anatase and rutile was calculated from the peak areas of the anatase and rutile peaks at 25.3° (2Θ) and 27.5° (2Θ), respectively.

The specific surface area of the photocatalysts was determined by nitrogen adsorption at 77 K using a Micromeritics gas adsorption analyzer (Gemini Type 2375). The specific surface area was calculated using the BET method.

The DR spectra of the samples (λ = 220–800 nm) were measured by a JASCO-V650 diode array computer controlled (SpectraManager Software) spectrophotometer with an integration sphere (ILV-724).

TEM micrographs were recorded on a Philips CM 10 instrument operating at 100 kV using Formvar coated copper grids.

A Horiba Jobin Yvon XGT-5000 X-ray fluorescent spectrometer, equipped with Rh X-ray source was used to measure the element content of the iodine doped titanium dioxide. The measurements were taken at an excitation voltage of 30 kV, an anode current of 0.5 mA and a measuring time of 1000 s.

X-ray photoelectron spectra of selected samples were taken with a SPECS instrument equipped with a PHOIBOS 150 MCD 9 hemispherical electron energy analyzer operated in the FAT mode. The excitation source was the Kα radiation of a magnesium anode ($h\nu$ = 1253.6 eV). Further details of the measurements are described elsewhere [35].

An Agilent 1100 series HPLC system equipped with Lichrospher RP 18 column followed the concentration of phenol, using a methanol/water mixture as the eluent (the detection was carried out at 210 nm).

The ESR experiments were carried out at room temperature using an ESP300E spectrometer (Bruker BioSpin, Germany), equipped with a standard rectangular mode TE_{102} cavity. After each illumination step for performing the ESR measurements, small aliquots of about 20 μL were transferred into 0.7 mm ID and 0.87 mm OD glass capillary tubes (VitroCom, NJ, USA), with a sample height of *ca.* 50 mm, and sealed on both ends with Cha-seal (Tube sealing compound, Chase Scientific Glass, Rockwood, TN, USA). To maximize the sample volume in the active zone of the ESR cavity, assemblies of seven tightly packed capillaries were bundled together and inserted into a wide-bore quartz capillary (standard ESR quartz tube with 2.9 mm ID and 4 mm OD, Model 707-SQ-250M, from Wilmad-LabGlass Inc., Vineland, NJ, USA). Such a setup resulted with *ca.* 140 μL sample volume in the active zone of the TE_{102} cavity, which, together with the division of the aqueous sample into seven physically separated volumes, markedly improved the overall sensitivity of measurements, as described [36,37]. The typical instrumental settings were: microwave frequency 9.77 GHz, microwave power 10.1 mW, sweep width 100 G, modulation frequency 100 kHz, modulation amplitude 0.5 G, receiver gain 2×10^4, time constant 81.92 ms, conversion time 40.96 ms and total scan time 41.9 s.

The overall scheme of the reactive scavenging of singlet oxygen by the diamagnetic compound, TMP-OH, and formation of the paramagnetic product, TEMPOL, is shown in Scheme 1. The overall scheme of the reactive scavenging of $OH^\bullet$ and $O_2^{\bullet -}$ radicals with the diamagnetic spin trap DMPO and formation of the paramagnetic spin-adducts DMPO-$OH^\bullet$ and DMPO-$OOH^\bullet$ is shown in Scheme 2.

2.3. Photocatalytic activity

2.3.1. Experiments in UV reactor system (Reactor I)

The UV photoreactor (Fig. 1) was an open Pyrex glass tube with double walls, surrounded by a thermostating jacket (25.0 °C). The reactor was irradiated by six fluorescent lamps (*Vilber-Lourmat T-6L* UV-A, 6W power, radiation maximum at 365 nm). The concentration of the photocatalyst in the suspension was 1 g/L, and

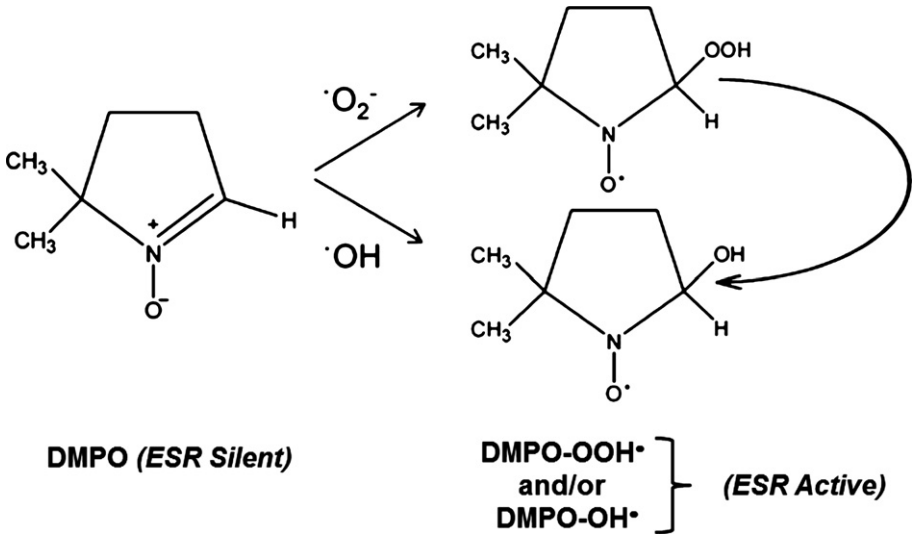

Scheme 2. Reactive scavenging of $OH^{\bullet}$ and $O_2^{\bullet -}$ radicals with DMPO.

0.5 mM phenol (Spektrum3D, 99.0%) solution was used as an example of contaminated water. The suspension (100 mL) was sonicated before the photocatalytic experiment. Whilst the experiment was in progress, a magnetic stirrer was used and air was bubbled through the liquid.

2.3.2. Experiments in Heraeus photoreactor system (Reactor II)

The VIS photoreactor (Fig. 1) was an immersion type *HERAEUS reactor* equipped with an *OSRAM* metal halide lamp (*Power Star HCl-TC 75W/WDL* type – visible light radiation) with $NaNO_2$ (Molar Chemicals, min. 99.13%) solution (1 M) in a thermostating jacket absorbing UV photons ($\lambda < 400$ nm). The concentration of the photocatalyst dispersion was 1 g/L, and 0.1 mM phenol solution was used to simulate contaminated water. The total volume was 400 mL and the presonicated suspension was stirred by magnetic stirrer and air was bubbled through it during the experiments.

2.3.3. Experiments in conventional 24 W energy saving compact fluorescence lamps equipped photoreactor (Reactor III)

For the disinfection experiments under visible light, the HERAEUS system (OSRAM metal halide lamp) was not applicable as the intensity of the light was too high and thus bacteria deactivation was observed by the irradiation without any titanium dioxide (possibly due to the inefficient filtering of the infrared part of the spectrum). Another special photoreactor was used for the disinfection experiments – an open glass vessel with double walls surrounded by a thermostating jacket at 25.0 °C. Around the reactor, four compact fluorescence lamps (DÜWI 25920/R7S-24W type – conventional 24 W energy saving compact fluorescence lamps) were mounted (Fig. 1), which type of light is widely used indoors. The light of the lamp was filtered by a circulating $NaNO_2$ aqueous solution (1 M) in the thermostating jacket to absorb UV photons below 400 nm, ensuring that only visible light was incident on the samples (the spectrum is shown in Fig. 2).

The comparison of the most active iodine doped titania and commercial titanium dioxides was carried out in this reactor system (Reactor III) by phenol decomposition and by killing *E. coli* bacteria. The titanias were purified before the experiments by centrifugation in 0.1 mM NaCl (Spektrum 3D, 99.0%) aqueous solution (three times at $c_{TiO_2} = 25.0$ g/L concentration), then the photocatalysts were resuspended in MilliQ water, dried at 80 °C and re-grinded in an agate mortar. The suspension (1 g/L TiO_2 in 100 mL of 0.9% NaCl solution) was ultrasonicated before the photocatalytic tests, and again during the experiments, a magnetic stirrer was used and air was bubbled through the liquid.

In the case of the phenol decomposition experiments, HPLC was used to measure the concentration of the substrate ($c_{0,phenol} = 0.1$ mM).

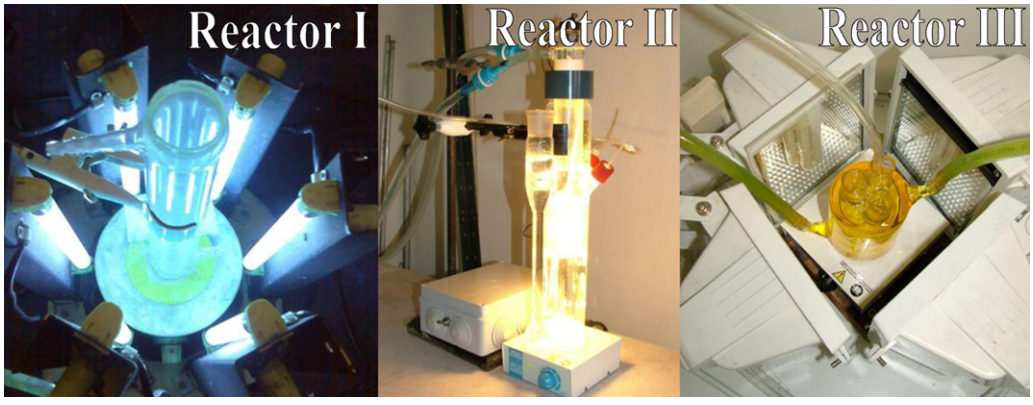

Fig. 1. Photographs of applied photoreactors: Reactor I – UV photoreactor system; Reactor II – Heraeus photoreactor system (VIS); Reactor III – photoreactor with conventional energy saving (24 W) compact fluorescence (VIS) lamps.

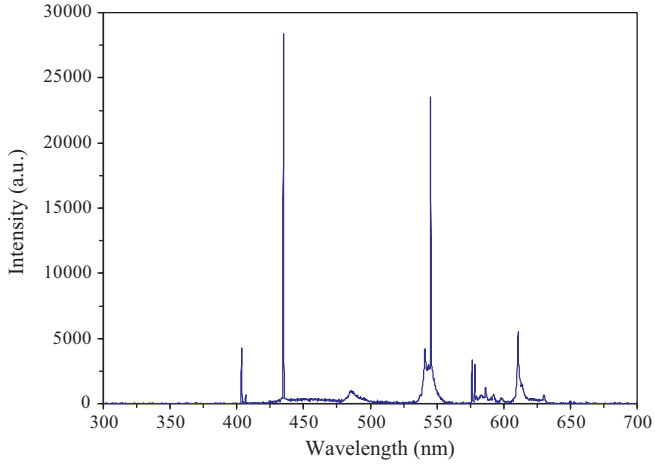

Fig. 2. Spectra of the conventional energy saving compact fluorescence lamps (24 W) with 1 M $NaNO_2$ light filtration.

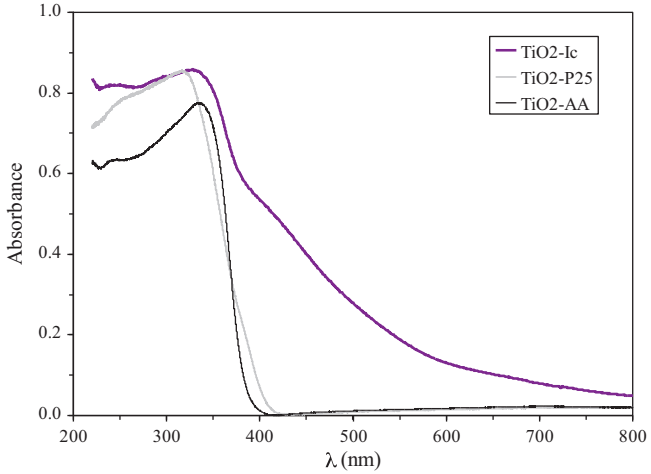

Fig. 3. DRS spectra of TiO_2-Ic; TiO_2-P25 and TiO_2-AA titania.

For the disinfection experiments, a suspension of *E. coli* was prepared by the inoculation of a 0.9% NaCl solution, which contained nutrients, such as 1% Tripton (Reanal, analytical grade) and 0.5% Yeast extract (Scharlau, analytical grade). It was incubated for 24 hours. Subsequently in order to eliminate the nutrients, the culture was washed twice with a 0.9% saline solution by centrifugation at 4000 rpm for 2 min, and the sediment was resuspended in 0.9% NaCl solution. From this bacteria suspension a calculated volume was added to the presonicated titanium dioxide suspension to set the initial colony forming unit to be 10^4 mL^{-1}. During the photocatalytic disinfection experiments, samples were plated on agar gels (Merck, analytical grade) and the grown colonies were counted after a 24 hour incubation at 37 °C in the dark. All of the samples were plated on 2 or 3 agar gels, ensuring the reliability of the data. All of the presented results were taken from the average of two parallel experiments.

3. Results and discussion

3.1. Characterization of the photocatalysts

TiO_2-P25 (Aeroxide P25), TiO_2-AA (Aldrich anatase) and the best iodine doped titanium dioxide (TiO_2-Ic) were characterized by several methods. Table 1 shows the particle size of the nanoparticles, the anatase and rutile content, the specific surface area, and the dopant content. TiO_2-Ic has the highest specific surface area (80 m^2/g), which can contribute to its high efficiency in photocatalytic processes [38]. All of the synthesized iodine doped titanium dioxides were characterized by X-ray diffraction (XRD) measurements which show that the main crystalline phase is anatase (98–100%), and the particle size was increasing by increasing the amount of added iodic acid (D = 8–24 nm).

The light absorption spectra were measured by a diffuse reflectance spectrophotometer and are illustrated in Fig. 3. It is obvious from the figure that iodine doped titania absorbs photons in the visible light range in contrast with pure Aldrich anatase and Aeroxide P25. However it should be noted that P25 contains 10 wt% rutile phase which can absorb some photons between 400 and 420 nm.

TiO_2-Ic was also examined by transmission electron microscopy. It can be concluded from Fig. 4 that the size distribution is relatively broad for the TiO_2-Ic sample (D = 3–24 nm). It can be also seen from the figure that this sample contains a significant amount of polyhedral particles. Our earlier studies confirmed that polyhedral particles are more active than spherical ones under UV irradiation [39,40], therefore this can contribute to the high efficiency of this sample.

The XPS spectrum of TiO_2-Ic shows that the sample has 0.67 at% iodine (expressed as $n_{Dopant}/n_{total} \times 100$) on the surface of the titanium dioxide particles. The oxidation states of iodine are I^- [19] (I $3d_{5/2}$ peak at 620.0 eV, 61%) and I^{7+} [19,28] (I $3d_{5/2}$ peak at 624.2 eV, 39%) (see Fig. 5).

By XRF measurements it was determined that the 0.5 n_I/n_{Ti} ratio of TiO_2-Ic sample underwent a drastic reduction during the calcination and the produced iodine doped titanium dioxide contains

Table 1
Structural parameters of the investigated photocatalysts (phase content, particle size, specific surface area and the concentration of dopant).

Sample	TiO_2-P25	TiO_2-AA	TiO_2-Ic
Anatase (wt%)[c]	90	100	98
Rutile (wt%)[c]	10	–	2
D_A (nm)	25.4	>85	9.0
D_R (nm)	~40	–	n.d.
Dopant content (at%)[d]	–	–	1.57[a]/0.67[b]
a_{BET}^S (m^2/g)	49	9.9	80

[a] Measured by XRF.
[b] Estimated by XPS.
[c] The weight percent of the crystalline phase of the sample.
[d] Expressed as $n_{Dopant}/n_{total} \times 100$.

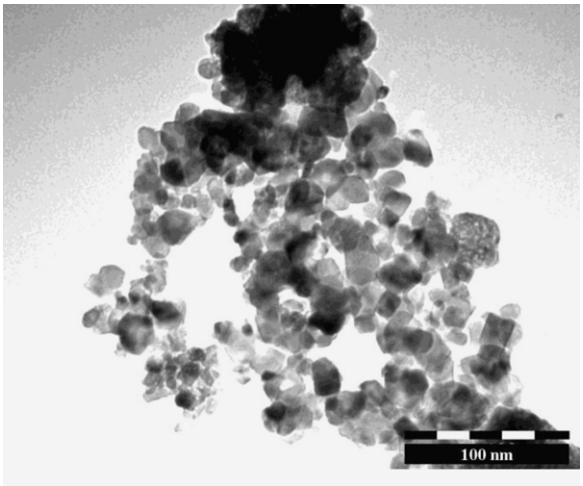

Fig. 4. TEM image of TiO_2-Ic.

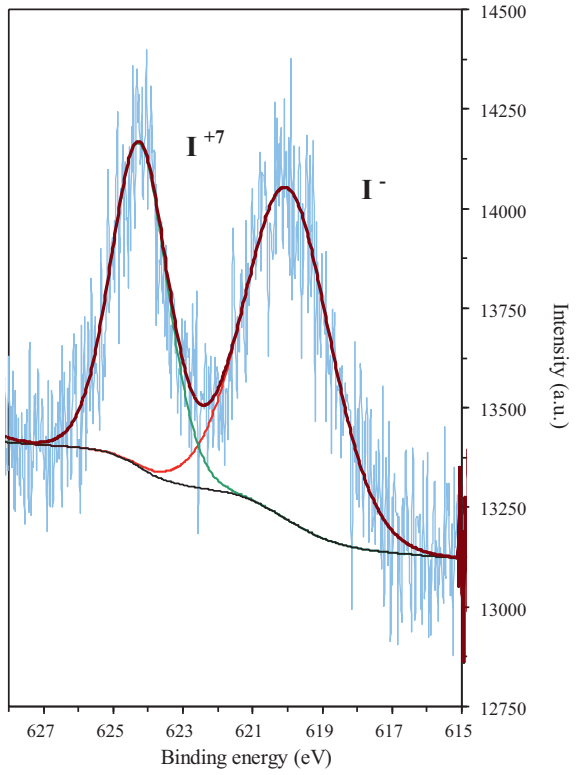

Fig. 5. XPS spectra of TiO_2-Ic (I $3d_{5/2}$).

only 1.57 at% iodine (expressed as $n_D/n_{total} \times 100$, this means that n_I/n_{Ti} is 0.048 in the calcinated photocatalyst).

3.2. Phenol degradation in Reactor I and Reactor II

The efficiencies of the iodine doped titanium dioxides for phenol decomposition were determined under UV and VIS irradiations. Fig. 6 demonstrates the decay curves under visible light irradiation. The initial degradation rates (r_0) were determined by the slope of the fitted linear trendline of the data points in the first hour of irradiation. The initial degradation rates are presented in Fig. 7. The determined r_0 values of the UV experiments are also presented in this figure and it demonstrates that the TiO_2-Ic sample had the highest efficiency in both cases of irradiation. Under VIS irradiation

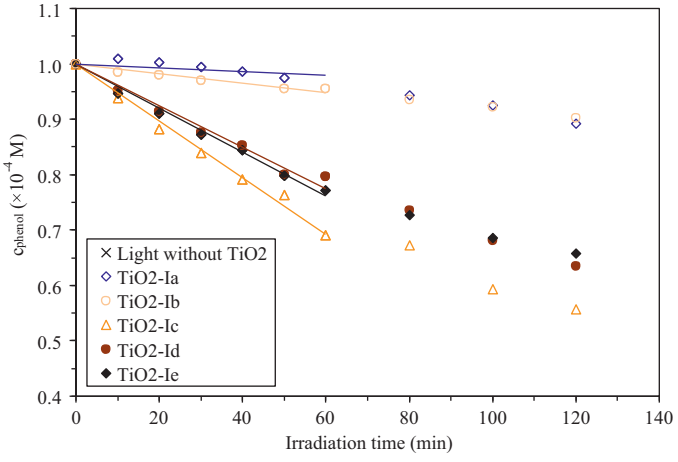

Fig. 6. Decay curves of phenol degradation experiments by VIS irradiated (Reactor II – Heraeus photoreactor system) iodine doped titanium dioxide series. The initial reaction rates are shown for all photocatalysts in Fig. 7.

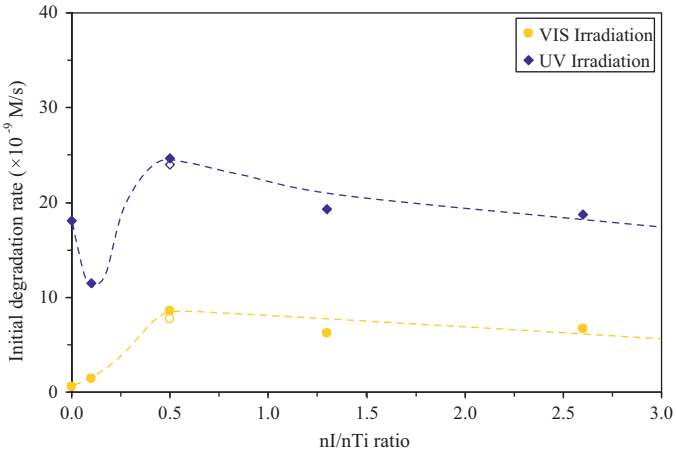

Fig. 7. Initial degradation rates of phenol under UV and VIS light irradiation in Reactor I and in Reactor II.

TiO_2-Ic,d,e samples showed similar efficiencies, but considering the results of the UV experiments, and the lower iodic acid consumption, the TiO_2-Ic sample has the most favourable properties. This champion iodine doped photocatalyst was re-synthesized and the measured photocatalytic activities were very similar (data points with empty symbols are shown in Fig. 7).

3.3. Phenol degradation and disinfection in Reactor III

In Reactor III, the TiO_2-Ic sample was compared with Aeroxide P25 (TiO_2-P25) and with Aldrich anatase (TiO_2-AA, which was applied as a reference TiO_2 with no VIS activity) by the decomposition of phenol, and by the inactivation of *E. coli* under visible light irradiation. The phenol decay curves are presented in Fig. 8. There was no decrease in the concentration under irradiation in the absence of the photocatalyst. In the case of Aldrich anatase there was an insignificant degradation observed (less than 5%). It appears from this figure, that iodine doped titania was about three times more efficient than TiO_2-P25. After four hours of irradiation TiO_2-Ic decomposed 57% of the phenol, with a 4.16×10^{-9} M/s initial degradation rate (data were fitted for 240 min), whilst TiO_2-P25 degraded only 17% of the phenol with a 1.23×10^{-9} M/s initial degradation rate. The high performance can be explained by the possibility of the activation with higher efficiency under VIS irradiation due to the successful doping method. The high specific surface area can

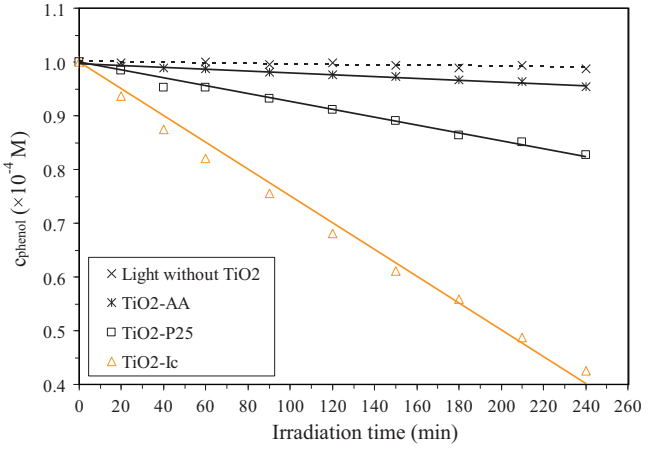

Fig. 8. Decay curves of phenol under VIS irradiation (Reactor III with conventional 24 W energy saving compact fluorescence lamps).

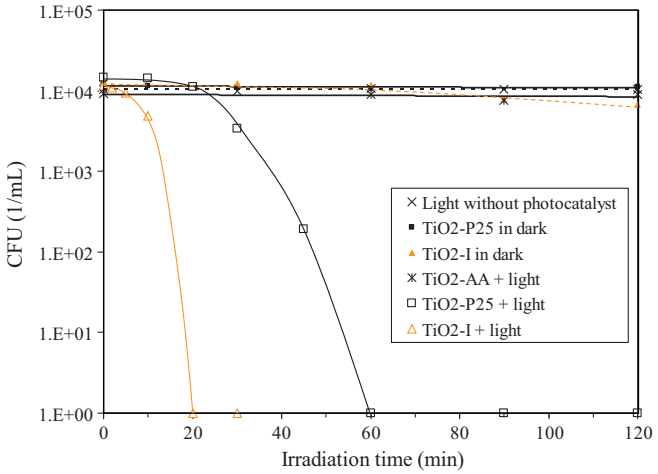

Fig. 9. Results of disinfection experiments under VIS irradiation (Reactor III with conventional 24 W energy saving compact fluorescence lamps).

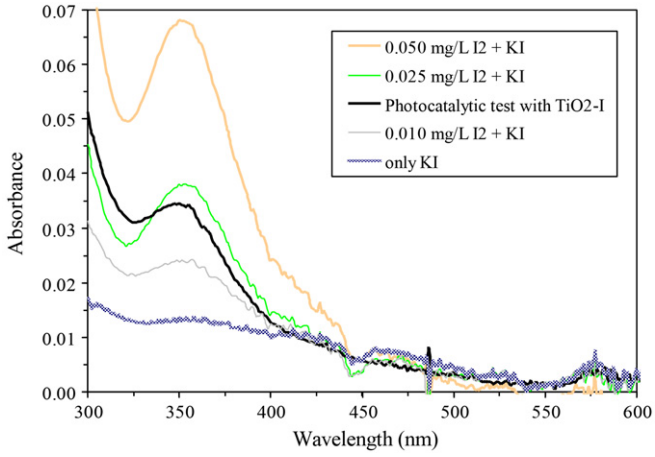

Fig. 10. Dissolved iodine detection by the formation of I_3^- with potassium iodide addition.

also contribute to the observed high phenol degradation efficiency [38].

The results of the disinfection experiments are illustrated in Fig. 9. All of the experiments were repeated twice, and the averages are illustrated on the figure. There was no CFU reduction under irradiation without any titanium dioxide or with TiO_2-AA. Applying TiO_2-P25, the colony forming unit was reduced to zero in one hour. TiO_2-Ic had much higher activity for the inactivation of *E. coli*, which totally sterilized the water in 20 min (Fig. 9).

Experiments were carried out to exclude the possibility that the determined disinfection effects were resulted by toxic compounds dissolved from the irradiated photocatalysts. Suspensions of the titanias (without bacteria) were irradiated for the amount of time at which they disinfected the solution in the previous experiments. The nanoparticles were then separated by centrifugation and filtration. After the separation, the colony forming unit was set to be 10^4/mL in this solution by the addition of *E. coli*, and it was poured back into the photoreactor. The CFU values were measured over 2 hours of irradiation and no notable CFU reduction was observed.

Since elemental iodine is highly volatile and the suspension was purged by air in the above described test, another experiment was also carried out with TiO_2-Ic without purging the suspension (and in this experiment bacteria were added to the suspension at the beginning). It is well known that activated titania can generate elemental iodine from iodide [41,42] and since, on the surface of the photocatalyst, 61% of the iodine total takes the form of I^-, the generation of I_2 is possible. After 20 min of irradiation, the suspension was centrifuged and the nanoparticles and bacteria were filtered out by a nanofilter. Subsequently, potassium iodide was added allowing the elemental iodide to form tri-iodide (I_3^-) ions which can then be detected spectrophotometrically at 360 nm [43]. Fig. 10 demonstrates that a trace amount of dissolved I_2 was detected in the solution after 20 min of irradiation (l = 10 cm). To determine the concentration of dissolved iodine, a calibration series (Fig. 10) was prepared (potassium iodide was added to 0.01–0.05 mg/L dissolved I_2 containing saline solutions, $c_{KI,final}$ = 39.4 mmol/L). There was approximately 0.010–0.025 mg/L dissolved elemental iodine in the solution after the photocatalytic test and the filtering procedure in case of the non-purged TiO_2-Ic suspension.

Iodine has a well-known antibacterial property [44,45]. To determine the effect of the dissolved iodine on the overall disinfection efficiency observed, a series of saline solutions containing I_2 in different concentration was produced. Fig. 11 shows the survival percentage of the bacteria in these solutions. 0.03 mg/L of dissolved iodine killed 53% of the bacteria. This means that the dissolved iodine produced from the TiO_2-Ic upon irradiation may have partially contributed to the high disinfection performance of this sample. The detected 0.010–0.025 mg/L dissolved elemental iodine can deactivate a maximum of 50% of the bacteria (Fig. 11) since in contrast to the photocatalytic experiment where the suspension was purged by air, this concentration was measured in an un-purged suspension. The purging of the system can result in lower elemental iodine concentration since it is highly volatile. It is also possible that the dissolved iodine may have participated in the phenol oxidation.

3.4. ESR measurements

Electron spin resonance (ESR) was used to follow the formation of the photo-sensitized reactive oxygen species (ROS) in this study. This approach used two distinct diamagnetic scavengers of reactive oxygen species (ROS): a 10 mM concentration of 2,2,6,6-tetramethyl-4-piperidinol (TMP-OH) and a 50 mM concentration of 5,5-dimethyl-1-pyrroline N-oxide (DMPO). The solutions of the ROS scavengers were prepared either in H_2O or in deuterated water (D_2O), mixed with TiO_2-Ic to form homogeneous suspensions, and illuminated with visible light in Reactor III. The final concentration of TiO_2-Ic in these suspensions was of 1.0 g/L and the total volume was 20 mL. The suspensions were sonicated before the ESR measurements for 5 min. Then, during the illumination experiments,

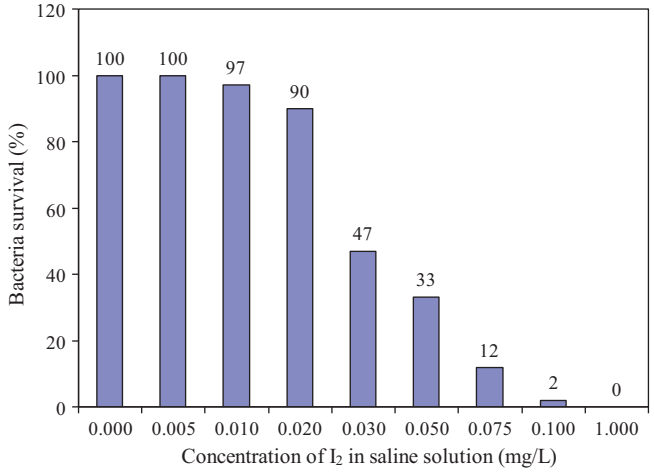

Fig. 11. Survival percentage of *E. coli* in the series of saline solutions containing I_2 in different concentration.

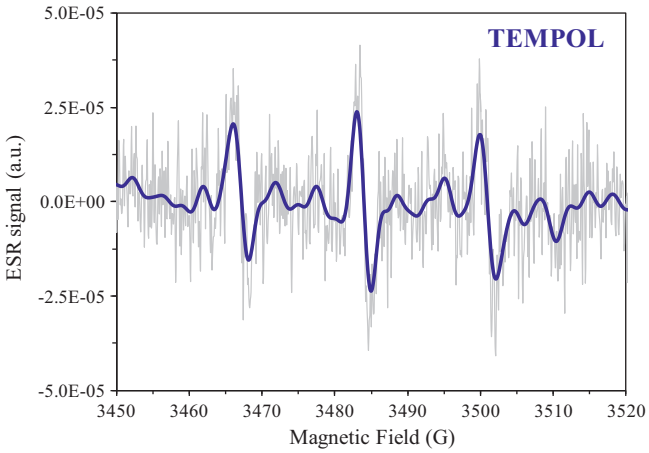

Fig. 12. ESR signal of TEMPOL.

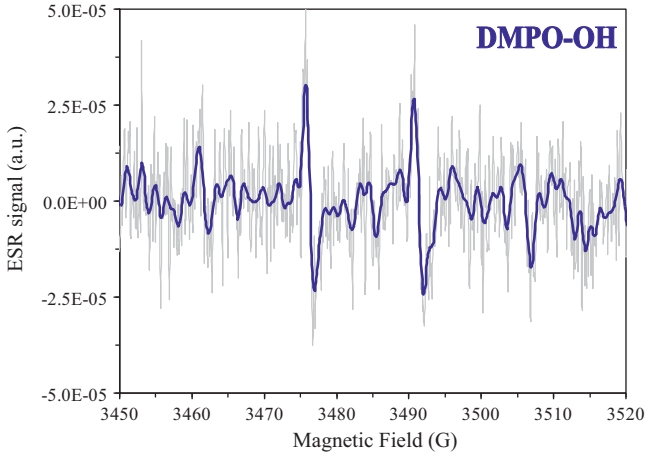

Fig. 13. ESR signal of DMPO-OH•.

the suspensions were vigorously stirred with the magnetic stirrer and air was bubbled through them. TMP-OH, DMPO and D_2O (isotopic purity of 99.9 at% D) were purchased from Sigma–Aldrich (Switzerland) and used as received.

In the presence of the TMP-OH radical scavenger and the VIS irradiated TiO_2-Ic suspension, an ESR signal of the paramagnetic product, 4-hydroxy-2,2,6,6-tetramethylpiperidine-1-oxyl (TEMPOL), was observed after 30 min of irradiation (Fig. 12). TEMPOL can be produced by the attack of singlet oxygen ($^1O_2$) or hydroxyl radicals (OH•) on TMP-OH [46]. In D_2O, the ESR signal of TEMPOL disappeared. This suggests that the generation of TEMPOL was mostly caused by OH•, since it is known that the presence of D_2O suppresses the formation of OD• radicals at the interface TiO_2/D_2O [47,48].

In the presence of the DMPO scavenger, a measurable DMPO-OH• signal (in H_2O) was observed under irradiation. This also proved the OH• radical generation on this titania (Fig. 13). Since no DMPO-OOH signal was detected, the iodine doped titania does not produce $O_2^{\bullet -}$ radicals in a measurable quantity.

4. Conclusions

A series of iodine doped titanium dioxide samples were synthesized with different iodine/titanium molar ratios during the synthesis. The optimum was determined by phenol degradation under UV and VIS irradiations and was found to be at 0.50.

The iodine doped titanium dioxide studied in this work had a much higher efficiency in phenol degradation and killing *E. coli* bacteria than the well-established industrial photocatalyst Aeroxide P25. To the best of our knowledge this is the first study of the disinfection efficiency of solely iodine-doped titanium dioxide under visible light irradiation.

The performed experiments proved that some elemental iodine was produced by the irradiated titanium dioxide. Dissolved iodine could have participated in the phenol oxidation and also contributed to the disinfection effects. Our study is the first to demonstrate this property of iodine doped titanias.

The high sterilization performance of the iodine doped sample may be partially a consequence of the formation of elemental iodine at very low concentrations and the photocatalytically generated OH• radicals, which were detected by ESR measurements.

Acknowledgements

This work was partially financed by the European Union through the Hungary-Serbia IPA Cross-border Co-operation Program, HU-SRB/0901/121/116. This work was also co-financed by the grant from the Hungarian National Office of Research and Technology (OTKA CK 80193) and the Swiss Contribution (SH/7/2/20). KM thanks the financial support of the Hungarian Research Foundation (OTKA PD78378) and the János Bolyai Research Scholarship of the Hungarian Academy of Sciences. A.S. and L.F. acknowledge the financial support of the Swiss National Science Foundation through the Nano-Tera NTF project “Core-shell superparamagnetic and upconverting nano-engineered materials for biomedical applications – NanoUp”.

The authors are indebted to Evonik Industries for supporting our work by supplying Aeroxide P25 titanium dioxide for these studies.

References

[1] C. Hu, J. Guo, J. Qu, X. Hu, Langmuir 23 (2007) 4982–4987.
[2] S. Malato, P. Fernández-Ibáñez, M.I. Maldonado, J. Blanco, W. Gernjak, Catalysis Today 147 (2009) 1–59.
[3] S. Song, J.J. Tu, Z.Q. He, F.Y. Hong, W.P. Liu, J.M. Chen, Applied Catalysis A 378 (2010) 169–174.
[4] X. Hong, Z. Wang, W. Cai, F. Lu, J. Zhang, Y. Yang, N. Ma, Y. Liu, Chemistry of Materials 17 (2005) 1548–1552.
[5] J.A. Rengifo-Herrera, J. Kiwi, C. Pulgarin, Journal of Photochemistry and Photobiology A 205 (2009) 109–115.
[6] J.A. Rengifo-Herrera, K. Pierzchała, A. Sienkiewicz, L. Forró, J. Kiwi, C. Pulgarin, Applied Catalysis B 88 (2009) 398–406.
[7] P. Wu, J.A. Imlay, J.K. Shang, Biomaterials 31 (2010) 7526–7533.
[8] P. Wu, R. Xie, J.A. Imlay, J.K. Shang, Applied Catalysis B 88 (2009) 576–581.
[9] Z. Pap, L. Baia, K. Mogyorosi, A. Dombi, A. Oszko, V. Danciu, Catalysis Communications 17 (2011) 1–7.
[10] K. Nagaveni, G. Sivalingam, M.S. Hegde, G. Madras, Environmental Science and Technology 38 (2004) 1600–1604.
[11] Z. Ambrus, N. Balazs, T. Alapi, G. Wittmann, P. Sipos, A. Dombi, K. Mogyorosi, Applied Catalysis B 81 (2008) 27–37.
[12] E.G. Bajnoczi, N. Balazs, K. Mogyorosi, D.F. Sranko, Z. Pap, Z. Ambrus, S.E. Canton, K. Noren, E. Kuzmann, A. Vertes, Z. Homonnay, A. Oszko, I. Palinko, P. Sipos, Applied Catalysis B 103 (2011) 232–239.
[13] J.C. Yu, W. Ko, J. Yu, H. Yip, P.K. Wong, J. Zhao, Environmental Science and Technology 39 (2005) 1175–1179.
[14] G. Liu, Z. Chen, C. Dong, Y. Zhao, F. Li, G.Q. Lu, H.M. Cheng, Journal of Physical Chemistry B 110 (2006) 20823–20828.
[15] Z.Q. He, C. Wang, H.Y. Wang, F.Y. Hong, X.H. Xu, J.M. Chen, S. Song, Journal of Hazardous Materials 189 (2011) 595–602.
[16] Z.Q. He, L.Y. Zhan, F.Y. Hong, S. Song, Z.Y. Lin, J.M. Chen, M.T. Jin, Journal of Environmental Sciences-China 23 (2011) 166–170.
[17] S. Usseglio, A. Damin, D. Scarano, S. Bordiga, A. Zecchina, C. Lamberti, Journal of the American Chemical Society 129 (2007) 2822–2828.
[18] S. Song, J.J. Tu, L.J. Xu, X. Xu, Z.Q. He, J.P. Qiu, J.G. Ni, J.M. Chen, Chemosphere 73 (2008) 1401–1406.
[19] W.Y. Su, Y.F. Zhang, Z.H. Li, L. Wu, X.X. Wang, J.Q. Li, X.Z. Fu, Langmuir 24 (2008) 3422–3428.
[20] S. Tojo, T. Tachikawa, M. Fujitsuka, T. Majima, Journal of Physical Chemistry C 112 (2008) 14948–14954.
[21] G. Liu, C.H. Sun, X.X. Yan, L. Cheng, Z.G. Chen, X.W. Wang, L.Z. Wang, S.C. Smith, G.Q. Lu, H.M. Cheng, Journal of Materials Chemistry 19 (2009) 2822–2829.

[22] J.F. He, Q.H. Liu, Z.H. Sun, W.S. Yan, G.B. Zhang, Z.M. Qi, P.S. Xu, Z.Y. Wu, S.Q. Wei, Journal of Physical Chemistry C 114 (2010) 6035–6038.
[23] X.F. Jiang, L. Yang, P. Liu, X. Li, J.A. Shen, Colloids and Surfaces B: Biointerfaces 79 (2010) 69–74.
[24] H. Sun, S. Wang, H.M. Ang, M.O. Tadé, Q. Li, Chemical Engineering Journal 162 (2010) 437–447.
[25] G. Liu, C.H. Sun, L.Z. Wang, S.C. Smith, G.Q. Lu, H.M. Cheng, Journal of Materials Chemistry 21 (2011) 14672–14679.
[26] Y. Ma, J.W. Fu, X. Tao, X. Li, J.F. Chen, Applied Surface Science 257 (2011) 5046–5051.
[27] S. Song, C. Wang, F.Y. Hong, Z.Q. He, Q.L. Cai, J.M. Chen, Applied Surface Science 257 (2011) 3427–3432.
[28] W.A. Wang, Q.A. Shi, Y.P. Wang, J.L. Cao, G.Q. Liu, P.Y. Peng, Applied Surface Science 257 (2011) 3688–3696.
[29] Q. Zhang, Y. Li, E.A. Ackerman, M. Gajdardziska-Josifovska, H. Li, Applied Catalysis A: General 400 (2011) 195–202.
[30] Z.Q. He, X. Xu, S. Song, L. Xie, J.J. Tu, J.M. Chen, B. Yan, Journal of Physical Chemistry C 112 (2008) 16431–16437.
[31] Z.Q. He, L. Xie, J.J. Tu, S. Song, W.P. Liu, Z.W. Liu, J.Q. Fan, Q. Liu, J.M. Chen, Journal of Physical Chemistry C 114 (2010) 526–532.
[32] S. Song, F.Y. Hong, Z.Q. He, H.Y. Wang, X.H. Xu, J.M. Chen, Applied Surface Science 257 (2011) 10101–10108.
[33] R.G. Nair, J.K. Roy, S.K. Samdarshi, A.K. Mukherjee, Colloids and Surfaces B: Biointerfaces 86 (2011) 7–13.
[34] T. Shirai, T. Shimizu, K. Ohtani, Y. Zen, M. Takaya, H. Tsuchiya, Acta Biomaterialia 7 (2011) 1928–1933.
[35] Z. Pap, V. Danciu, Z. Cegléd, Á. Kukovecz, A. Oszkó, A. Dombi, K. Mogyorósi, Applied Catalysis B 101 (2011) 461–470.
[36] Y.E. Nesmelov, D.D. Thomas, Journal of Magnetic Resonance 178 (2006) 318–324.
[37] J.I. Nieto-Juarez, K. Pierzchla, A. Sienkiewicz, T. Kohn, Environmental Science and Technology 44 (2010) 3351–3356.
[38] S. Kim, W. Choi, Journal of Physical Chemistry B 109 (2005) 5143–5149.
[39] N. Balazs, K. Mogyorosi, D.F. Sranko, A. Pallagi, T. Alapi, A. Oszko, A. Dombi, P. Sipos, Applied Catalysis B 84 (2008) 356–362.
[40] N. Balazs, D.F. Sranko, A. Dombi, P. Sipos, K. Mogyorosi, Applied Catalysis B 96 (2010) 569–576.
[41] C. Karunakaran, S. Senthilvelan, S. Karuthapandian, K. Balaraman, Catalysis Communications 5 (2004) 283–290.
[42] C. Karunakaran, P. Anilkumar, Journal of Molecular Catalysis A: Chemical 265 (2007) 153–158.
[43] Y. Nishiyama, M. Terazima, Y. Kimura, Chemical Physics Letters 491 (2010) 164–168.
[44] G.M. Brion, J. Silverstein, Water Research 33 (1998) 169–179.
[45] S. Punyani, P. Narayana, H. Singh, P. Vasudevan, Journal of Scientific and Industrial Research 65 (2006) 116–120.
[46] I. Rosenthal, C.M. Krishna, G.C. Yang, T. Kondo, P. Riesz, FEBS Letters 222 (1987) 75–78.
[47] J. Cunningham, S. Srijaranai, Journal of Photochemistry and Photobiology A 43 (1988) 329–335.
[48] P.K.J. Robertson, L.A. Lawton, B. Cornish, M. Jaspars, Journal of Photochemistry and Photobiology A 116 (1998) 215–219.